AUT Journal of Mechanical Engineering

AUT J. Mech. Eng., 5(3) (2021) 343-360
DOI: 10.22060/ajme.2021.18654.5910

Effects of gas temperature rise on steady state behavior of non-circular two-lobe micro gas bearings

A. Gharanjik, A. Karami mohammadi*

Faculty of Mechanical Engineering, Shahrood University of Technology, Shahrood, Iran

ABSTRACT: In this paper, the molecular gas lubrication model is used to analyze the steady state behavior of two-lobe non-circular gas lubricated micro bearings. In this way, the effects of increasing temperature and gas rarefaction can be considered and then examined and analyzed. Behavior characteristics of two-lobe non-circular bearings with very small sizes differ from conventional sizes, especially at high temperatures and/or high rotational speeds. At high temperatures, in addition to diluting the gas, its viscosity and friction also change, and slippage may occur at the boundaries. The nonlinear equation governing the behavior of the gas is discretized using the finite element method and then solved together with the static equations of the rotor. Then the effects of temperature increase and gas rarefaction on gas pressure profile, load bearing capacity, angle of attitude, eccentricity ratio and frictional power loss have been studied and analyzed. The results show that the temperature rise and the gas rarefaction have significant effects on the steady state behavior of micro gas bearings. Among the results is that with increasing gas rarefaction, the gas pressure and consequently the load carrying capacity decrease more, and the attitude angle also increases more.

Review History:

Received: Jun. 30, 2020
Revised: Jan, 09, 2021
Accepted: Jan, 09, 2021
Available Online: Jan, 11, 2021

Keywords:

Non-circular two-lobe micro gas bearings
Gas temperature rise
Gas rarefaction
molecular gas lubrication model, inverse Knudsen number

1- Introduction

Micro-bearings are an important component of micro-electromechanical power systems such as micro-motors and have received much attention today. To increase power, the rotor must work at a very high speed. In order to design high-reliability rotary devices and prevent hazardous performance at such high speeds, it is best to have an accurate prediction of system behavior. Due to the small size of the micro-gas bearings, the thickness of the gas film is comparable to the molecular free path. At this scale, the fluid mechanics of these bearings are very different from those of large-scale bearings, and this difference affects the performance of the bearing. Due to the high rotor speed and high temperature, the distance between the surface of the rotor and the bearing surface is reduced to about a few microns. Also, the gas film between them is rarefied as well as the speed slip occurs at the rotor surface. Thus, the velocity distribution in the gas film changes and in turn affects the performance of the micro-bearing. To determine the pressure and force distribution in the lubricant gas film, the governing equation in accordance with the molecular gas lubrication (MGL)model, along with the velocity-slip boundary conditions must be solved.

In 1999, Piekos and Breuer studied the stability of a hydrodynamic journal bearing in a gas micro turbine using pseudo-spectral orbit simulations. By comparing the solution of the Navier Stokes equations and the Reynolds equation, the Reynolds equations are valid for analyzing journal bearing with a gas lubricant in the gas micro turbine [1]. In 2004, Kim et al. made micro-gas bearings with lithography and deep X-rays electroplating and calculated the performance of micro-bearings in terms of load parameters and angles of attitude using the MGL theory [2].

Of the main disadvantages of gas bearings are low stability, which often limits their range of applications. In 2005, Isomura et al. designed and developed a high speed micro bearing for conducting experiments to continue developing air bearings for a micro turbine capable of stability operating at 870000 rpm [3]. In 2006, Arghir et al. dealt with several aspects of the finite-volume numerical solution of the Reynolds equation for a compressible fluid. The static and dynamic characteristics of cylindrical hydrodynamic and externally pressurized hybrid gas bearings are presented[4]. In 2009, Zhang derived a new slip model by molecular dynamics to investigate the ultra-thin gas lubricated slider bearings. He obtained analytical solutions for flow rate, pressure distribution, load carrying capacity and stream wise location using the modified Reynolds equation [5]. Zhang et al. analyzed the characteristics of gas journal micro-bearings based on effective viscosity according to first-order slip boundary conditions [6]. In 2010, Zhang et al. proposed a modified Reynolds equation based on Burgdorfer's first order slip boundary conditions at different

*Corresponding author's email: akaramim@shahroodut.ac.ir

temperatures. Their numerical analysis showed that gas film pressure and dimensionless load carry capacity decreased significantly when increasing the gas rarefaction effect [7]. Zhang et al. analyzed the static performance of micro-bearings using spectral correlation methods. The results show that load carrying capacity increases with lower operating temperatures, and the dependence of temperature on load capacity at higher temperatures becomes weaker [8]. In 2013, Zhang et al. coupled the gas film lubrication equation with kinetic equations to study the characteristics of rotor-bearing systems. They found that the temperature range can be divided into two regions: the area with the dominant viscosity and the area with the dominant rarefaction effect [9]. In 2015, Yan et al. a modified Reynolds equation for bump type gas foil thrust bearing established with consideration of the gas rarefaction coefficient. Under rarefied gas lubrication, the Knudsen number which was affected by the film thickness and pressure was introduced to the Reynolds equation. The coupled modified Reynolds and lubricating film thickness equations were solved using Newton-Raphson iterative method and finite difference method. By calculating the load capacity for increasing rotor speeds, the lift-off speed under certain static load was obtained. Parametric studies for a series of structural parameters and assembled clearances were carried out for bearing optimization design. The results indicate that with gas rarefaction effect, the axial load capacity would be decreased, and the lift-off speed would be improved. The rarefied gas has a more remarkable impact under a lower rotating speed and a smaller foil compliance coefficient [10]. In 2016, Zhang et al. extracted the first-order modified Reynolds equation with respect to thermal creep, which led to a very high thermal gradient in the axial direction, and was compared with the simplified energy equation for examination of the hydrodynamic characteristics of the steady state of micro gas-bearing were coupled. Under the iso-thermal conditions, they realized that carbon dioxide gas could not only improve the bearing's stability but could also produce a relatively higher load carrying capacity [11]. Chen et al. analyzed pressure distribution, capacity, and stiffness of the gas film under the rarefied effect in the aerostatic thrust bearing. With the increase of gas pressure, the gas film capacity and stiffness of bearing would also increase [12]. Liangliang Li et al. investigated the sensitivity of MEMS gas bearing performance to the wear in different axial and circumferential positions in detail. Rarefaction effect is considered into the transient and steady lubrication equation, and then the finite element method (FEM) is employed to solve the equations. The static and dynamic characteristics of the bearing in 50 wear conditions are calculated for each case [13]. Yao Wu et al. investigated elastic deformation and gaseous rarefaction effects in the pressure distribution and dynamic stiffness and damping coefficients and also friction coefficient. They used the effective viscosity model of Veijola, finite element procedure and relaxed iterative algorithm. They showed elastic deformation and gaseous rarefaction effects have great importance in the static and dynamic behavior of gas micro bearings[14]. Yao Wu et al. derived the modified Reynolds equations including different rarefaction models and solved by the partial derivative method and relaxation iteration algorithm. They investigated the effects of Knudsen number and bearing parameters on the static and dynamic characteristics of micro bearings . They showed that the rarefaction effect plays a crucial role in the ultra-thin gas film lubrication[15].

In 1975, Pinkus solved the compressible Reynolds equation under homogeneous conditions for elliptical and three-lobe gas bearings with a working load vector in any desired direction in a 360 degrees range. He showed that compared to conventional bearings, non-circular designs offer significant advances in stiffness [16]. In 1983, Chandra examined the static and dynamic characteristics of the four configurations of the non-circular gas journal bearings. Reynolds equation was solved by finite element method, and a comparison of the stability of four non-circular gas journal bearings was performed [17]. Saha et al. theoretically analyzed the steady state performance of gas-lubricated two-layered porous journal bearings by an iterative method considering three-dimensional flow through the porous matrix and two-dimensional flow in the bearing clearance. The effect of supply pressure, bearing number, feeding parameter and length-diameter ratio on the static characteristics are investigated and presented in the form of design charts [18]. Rahmatabadi et al. studied the static and dynamic characteristics of non-circular gas journal bearings, considering the effect of the angle of installation and pre-load. They have proven that non-circular bearings have better dynamic characteristics than circular bearings. They also proved that using the appropriate amount of mounting angles, the stability margin can be increased [19]. Crosby studied static and dynamic characteristics of two-lobe journal bearings lubricated with couple-stress fluids. The load carrying capacity, the stiffness and damping coefficients, the non-dimensional critical mass, and the whirl ratio are determined for various values of the couple stress parameter [20]. Rahmatabadi et al. investigated the effects of bearing preload factor on the static performance characteristics of micropolar lubricated two-, three-, and four-lobe bearings and solved the modified Reynolds equation for micropolar fluids by FEM, to find the fluid film pressure. Then, in turn, bearing performance characteristics, namely, load-carrying capacity, attitude angle, frictional force, friction coefficient, and side leakage flow were calculated [21]. Chauhan et al. carried out a comparative study based on the thermal performance of elliptical and offset-halves journal bearings. Investigation for the rise in oil film temperatures, thermal pressures, load capacity, and power loss for three commercially available grade oils have been carried out for bearing configurations under study [22]. Sharma et al. theoretically studied the influence of wear on the performance of a non-circular 2-lobe four-pocket multirecess hybrid journal bearing system. The Reynolds equation governing the flow of lubricant in the clearance space of a non-circular 2-lobe multirecess worn hybrid journal bearing system has been solved using FEM along with appropriate boundary conditions [23]. Shooroki

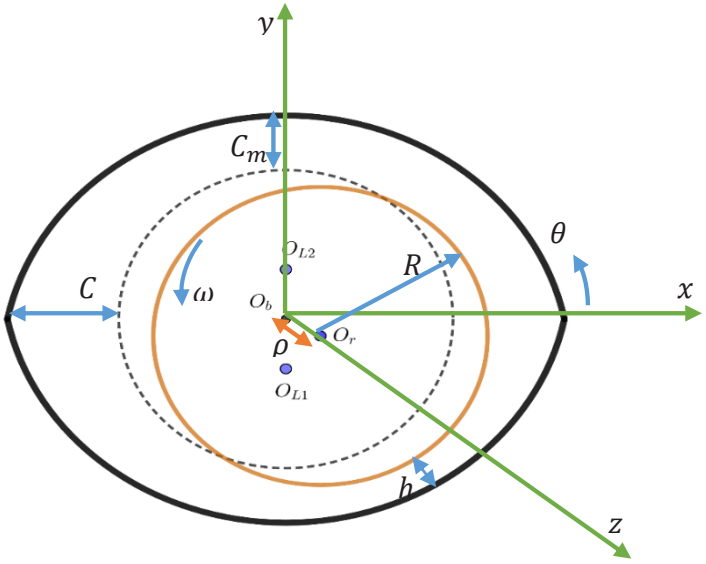

Fig. 1. Geometric details of the two-lobe non-circular micro gas bearings

et al. studied the static characteristics of two lobes, three lobes and four lobes non-circular gas bearing systems. They analyzed the Reynolds equation using radial basis functions. They used a numerical method to solve the system of algebraic equations and determined the position of the rotor equilibrium without using the trial and error method, which was considered as the advantage of their method [24]. Chen et al. numerically investigated static performance of the journal bearing with rectangular grooves . The resistance network method (RNM) was utilized to solve the Reynolds equation required in the analysis. Performance parameters including pressure distribution P, load force $\mathbf{F}$, stiffness K, and gas flow rate Q are examined in the simulations [25].

Due to the work done over the past decades, numerous studies have been carried out on non-circular gas-bearing on macro-scale, and the results have shown that non-circular gas bearings have better performance and stability than circular gas bearings. Therefore, considering the fact that in micro-scale and in micro-motors, despite the high speeds and high temperatures, the issue of stability has particular importance, it seems that the use of non-circular gas micro-bearings is a better option for such machines. Several studies have been carried out on micro gas bearings and their types, but no research work has been carried out on two lobes non-circular micro gas bearings, and its vacancy is tangible.

In this paper, we try to investigate the nonlinear steady state behavior of two lobes non-circular micro gas bearings. The molecular gas lubrication model has been used for steady state analysis of two-lobe non-circular micro gas bearings. The effects of temperature rise and gas rarefaction are taken into account. The nonlinear equation governing the gas behavior is discretized using the finite element method and then solved. The effects of temperature rise and gas rarefaction on pressure, micro bearing load carrying capacity, angle of attitude, eccentricity ratio, and frictional power loss have been studied. The results show that the temperature rise and the gas rarefaction have significant effects on micro gas bearings steady state behavior.

2- Problem definition and solution

2- 1- MGL model

The geometric details of the non-circular bearing of the two lobes are shown in Fig. 1. The analysis of two-lobe non-circular micro gas bearing consists of solving the governing equations separately for each bearing lobe. Each lobe is considered as an independent component of the bearing. To extend the analysis to the whole of the non-circular bearing, the gas film geometry of each lobe is expressed with reference to bearing fixed Cartesian axes. At operation, the minimum gas film thickness is about a few microns, which is sufficiently effective to compare the molecular mean free path. The conventional compressible Reynolds equation loses its validity as the governing equation. The modified Reynolds equations are obtained based on the first or second-order slip conditions based on the assumption that the small Knudsen number ($Kn = \frac{\lambda}{h} \ll 1$) is obtained, in while the MGL model obtained from the linearized Boltzmann equation, It is valid for all arbitrary Knudsen numbers. Therefore, this model has been used in the analysis of non-circular micro gas bearing. The assumptions considered are: flow is laminar and isothermal, inertia and body forces are negligible and there is no vertical flow across the film. The MGL model [26] is as follows:

$$\frac{\partial}{\partial\theta}\left[\left(PH^3Q\right)\frac{\partial P}{\partial\theta}\right]+\frac{\partial}{\partial\zeta}\left[\left(PH^3Q\right)\frac{\partial P}{\partial\zeta}\right]=\Lambda\frac{\partial}{\partial\theta}\left(PH\right) \tag{1}$$

where $\zeta=\frac{z}{R}$ is non-dimensional coordinate along bearing axis measured from mid span, $\theta=\frac{x}{R}$ is angular coordinate measured from X-axis, $P=\frac{p}{p_a}$ is non-dimensional absolute gas pressure, p_a is pressure at a reference position. Λ is bearing number and is as follow

$$\Lambda=\frac{6\mu\omega}{p_a}\left(\frac{R}{C_m}\right)^2 \tag{2}$$

that μ is gas dynamic viscosity, ω is rotational speed of the rotor, R is rotor radius and C_m is minor clearance when rotor and bearing geometric centers are coincident.

The non-dimensional gas film thickness (H) in the clearance space of the first or second lobe with the rotor in steady state can be expressed as

$$H=\frac{h}{C_m}=\frac{1}{\delta}-X_{j0}\cos\theta-Y_{j0}\sin\theta+\left(\frac{1}{\delta}-1\right)\cos\left(\theta-\theta_0^k\right) \tag{3}$$

that δ is preload in the bearing, $\left(X_{j0},Y_{j0}\right)$ is coordinates of the rotor center in steady state and θ_0^k is angle of lobe line of centers for kth Lobe.

The Q is non-dimensional flow rate coefficient corresponding to different degrees of rarefaction. $Q=1$ represents continuous flow, when gas flow is rarefied, it is more than 1, and is equal to the ratio of Q_p (flow rate coefficients of the rarefied Poiseuille flow) to Q_c (flow rate coefficients of the continuum Poiseuille flow). As follows:

$$Q=\frac{Q_p}{Q_c} \tag{4}$$

For Q_p and Q_c, Fukui and Kaneko[27] is given polynomial expressions proportional to numerical computation data for the flow coefficient by inverse Knudsen number, which are as follows:

$$\begin{cases} Q_c=\dfrac{D_k}{6} \\ Q_p=\dfrac{D_k}{6}+1.0162+\dfrac{1.0653}{D_k}-\dfrac{2.1354}{D_k^2}, & 5\le D_k \\ Q_p=0.13852D_k+1.25087+\dfrac{0.15653}{D_k}-\dfrac{0.00969}{D_k^2}, & 0.15\le D_k<5 \\ Q_p=-2.22919D_k+2.10673+\dfrac{0.01653}{D_k}-\dfrac{0.0000694}{D_k^2}, & 0.01\le D_k<0.15 \end{cases} \tag{5}$$

both Q_p and Q_c are related to inverse Knudsen number the (D_k), which changes with temperature as follow

$$D_k=\frac{ph}{\mu\sqrt{2R_gT}} \tag{6}$$

that T is temperature and R_g is gas constant.

The boundary conditions for solving Eq. (1) are as follows:

gas pressure on both sides of the bearing is equal to the ambient pressure. $P\left(\theta,\pm\frac{L}{D}\right)=1$

gas pressure P is continuous. $\left.\frac{\partial P}{\partial\zeta}\right|_{\zeta=0}=0$

The gas pressure at the leading and the trailing edges of each lobe is equal to the ambient pressure p_a.

2- 2- Finite element method

The MGL model is a nonlinear partial differential equation that can be solved using finite element method. For the formulation of finite element [28], the Galerkin's weighed residual of Eq. (1) for an element of the discretized space domain as follows:

$$\iint_{A^e}\left\{\frac{\partial}{\partial\theta}\left[\left(PH^3Q\right)\frac{\partial P^e}{\partial\theta}\right]+\frac{\partial}{\partial\zeta}\left[\left(PH^3Q\right)\frac{\partial P^e}{\partial\zeta}\right]-\Lambda\frac{\partial}{\partial\theta}\left(P^eH\right)\right\}N_i^e\,d\theta\,d\zeta=0 \tag{7}$$

here, N_i^e is approximation function and A^e is element area. In the discretized space domain, in an element e, the pressure variable P is approximated as follows:

$$P^e = \sum_{j=1}^{n_e} N_j^e P_j \tag{8}$$

in which e refers to an element, n_e the number of nodes in the element, N_j^e's are the shape functions, and P_j's are the nodal values of the pressure variable P. Using the Eq. (8) in Eq. (7) and with some integral simplifications, the finite element equations for an element of the discretized flow filed domain can be obtained as.

$$[K]^e \{P\}^e = \{V\}^e + \{B\}^e \tag{9}$$

in which the components of the element matrices are as:

$$\begin{cases} K_{ij}^e = \iint\limits_{A^e} \left(P^e H^3 Q \nabla N_j^e\right).\left(\nabla N_i^e\right) \\ V_i^e = \iint\limits_{A^e} \Lambda P^e H \dfrac{\partial N_i^e}{\partial \theta} d\theta d\zeta \\ B_i^e = \int\limits_{S^e} \left(P^e H^3 Q \dfrac{\partial P^e}{\partial \zeta}\right) N_i^e d\theta + \\ \qquad \int\limits_{S^e} \left(P^e H^3 Q \dfrac{\partial P^e}{\partial \theta} - \Lambda P^e H\right) N_i^e d\zeta \end{cases} \tag{10}$$

The assembly of Eq. (9) for all elements of P domain yields the global equations:

$$[K]_{n_k \times n_k} \{P\}_{n_k \times 1} = \{V\}_{n_k \times 1} + \{B\}_{n_k \times 1} \tag{11}$$

where n_k is the total number of nodes.

3- Performance characteristics

3- 1- equilibrium position of rotor center

For the given vertical load, the equilibrium position of the rotor center can be obtained by solving the following equations

$$\begin{cases} F_{gx}\left(X_{j0}, Y_{j0}\right) + F_{fx}\left(X_{j0}, Y_{j0}\right) + F_{ex} = 0 \\ F_{gy}\left(X_{j0}, Y_{j0}\right) + F_{fy}\left(X_{j0}, Y_{j0}\right) + F_{ey} = 0 \end{cases} \tag{12}$$

where F_{ex} and F_{ey} are the external force components, F_{gx} and F_{gy} are the gas film force components, and F_{fx} and F_{fy} are the viscous friction force components. By guessing the equilibrium position of the rotor center, Eq. (12) is solved using an iterative method and the equilibrium position of the rotor center $\left(X_{j0}, Y_{j0}\right)$ is obtained. The F_{gx} and F_{gy} are obtained using the following double integrals:

$$\begin{cases} F_{gx} = -\int\limits_{-\frac{L}{D}}^{\frac{L}{D}} \int\limits_{0}^{\pi} P\cos\theta d\theta d\zeta - \int\limits_{-\frac{L}{D}}^{\frac{L}{D}} \int\limits_{\pi}^{2\pi} P\cos\theta d\theta d\zeta \\ F_{gy} = -\int\limits_{-\frac{L}{D}}^{\frac{L}{D}} \int\limits_{0}^{\pi} P\sin\theta d\theta d\zeta - \int\limits_{-\frac{L}{D}}^{\frac{L}{D}} \int\limits_{\pi}^{2\pi} P\sin\theta d\theta d\zeta \end{cases} \tag{13}$$

L and D are the length and diameter of the bearing, respectively. Dual integrals of Eq. (13) are calculated by numerical methods and the gas film force is obtained. The dimensionless viscous friction force, F_f, can be calculated as follows:

$$\begin{cases} F_{fx} = \dfrac{1}{p_a}\left(\int\limits_{-\frac{L}{D}}^{\frac{L}{D}} \int\limits_{0}^{\pi} \tau_h \sin\theta d\theta d\zeta + \int\limits_{-\frac{L}{D}}^{\frac{L}{D}} \int\limits_{\pi}^{2\pi} \tau_h \sin\theta d\theta d\zeta\right) \\ F_{fy} = -\dfrac{1}{p_a}\left(\int\limits_{-\frac{L}{D}}^{\frac{L}{D}} \int\limits_{0}^{\pi} \tau_h \cos\theta d\theta d\zeta + \int\limits_{-\frac{L}{D}}^{\frac{L}{D}} \int\limits_{\pi}^{2\pi} \tau_h \cos\theta d\theta d\zeta\right) \end{cases} \tag{14}$$

τ_h is the shear stress caused by gas viscosity at the rotor surface, which can be calculated as follows [29]:

$$\tau_h = \frac{HC_m p_a}{2R}\frac{\partial P}{\partial \theta} + \frac{\mu\omega R}{C_m H} \tag{15}$$

3- 2- Load carrying capacity

Load carrying capacity is obtained as follows:

$$W_0 = \sqrt{F_{gx}^2 + F_{gy}^2} \tag{16}$$

3- 3- Attitude angle

The attitude angle of the journal center for a given eccentricity is determined by an iteration scheme. This scheme is based on minimization of the horizontal load component (F_x) so that the resultant load is almost vertical (i.e., $F = F_y$).

Table 1. Comparison of the results in steady state with the results of [17, 24] for L / D = 1, δ = 0.5

Λ	F_e	$X_{j0}{}^1$	$Y_{j0}{}^1$	$X_{j0}{}^2$	$Y_{j0}{}^2$	$X_{j0}{}^3$	$Y_{j0}{}^3$
0.1	0.01	0.244	-0.002	-	-	0.2402	-0.0027
0.5	0.05	0.242	-0.014	-	-	0.2381	-0.0145
1	0.1	0.236	-0.026	-	-	0.2311	-0.0280
2	0.2	0.217	-0.050	0.224	-0.053	0.2097	-0.0528
5	0.5	0.16	-0.103	0.166	-0.111	0.1524	-0.1073
10	1	0.126	-0.178	0.122	-0.174	0.1229	-0.1746
20	2	0.087	-0.272	-	-	0.086	-0.2705

1: The results of Chandra [17] 2: The results of Shooroki [24] 3: Present analysis

$$\Phi = \arctan\left(\frac{X_{j0}}{Y_{j0}}\right) \tag{17}$$

3- 4- Frictional power loss

The friction force for two-lobe non-circular micro gas bearing is computed from the following equation:

$$F_L = \frac{\bar{F}_L C_m}{\mu R^3 \omega} = \iint_A \left(\frac{3H}{\Lambda}\frac{\partial P}{\partial \theta} + \frac{1}{H}\right) d\theta d\zeta \tag{18}$$

The frictional power loss for the bearings is given by

$$P_L = \frac{\bar{P}_L C_m}{\mu R^4 \omega^2} = \iint_A \left(\frac{3H}{\Lambda}\frac{\partial P}{\partial \theta} + \frac{1}{H}\right) d\theta d\zeta \tag{19}$$

4- Result and Discussion

4- 1- Verification

To ensure the accuracy of the analysis and results, first assuming that no fraction occurs, i.e. at $Q = 1$ (continuous flow), the rotor equilibrium position is obtained and in table 1, with the results of Shuruki et al. [24] as well as Chandra et al. [17] is compared. Table 1 shows good agreement between the results.

Then, to ensure the accuracy of the results obtained on a micro-scale, since no work has been done on multi-lobe non-circular gas-lubricated micro-bearings, the steady-state characteristics of circular micro-bearings (one lobe) are obtained and compared with the results of Malik [30] in Table 2. According to Table 2, there is a good agreement between the obtained results and the results of Malik [30]. It is worth noting that the difference in $Kn=0$ is due to the larger number of elements (about 17,000 elements) in the present study, and the difference in the case of Kn=0.1 is due to the use of the modified first-order Reynolds equation in Malik's paper [30], while in this research the MGL model is used, which is more accurate than other models.

4- 2- Results

In this study, air is considered as a lubricant and bearing characteristics are as follows:

$$L/D = 0.1, \qquad p_a = 101325 Pa, \qquad \delta = 0.5$$

The non-dimensional peripheral pressure profile in the middle section of two-lobe non-circular micro gas bearing is presented in Figs. 2 to 4, in which the ratio of the length to diameter is 0.1 and the preload ($\delta = \frac{C_m}{C}$) is 0.5. The rotational speed of the rotor is 100,000, 500,000 and 1,000,000 rpm respectively. The results show that increasing the temperature has a significant effect on the pressure characteristics so that the pressure values in the pressure characteristics increase. However, when the effect of gas rarefaction is considered, the pressure values in the pressure characteristics are reduced relative to the case in which the gas rarefaction is ignored. Also, increasing the gas temperature increases the viscosity of the gas, which in turn increases the gas pressure.

Fig. 2 shows the pressure profile when the rotational speed of the rotor is 100,000 rpm in two cases. When the effect of gas rarefaction is considered, the pressure values decrease.

Table 2. Comparison of results in steady state for circular micro gas bearing (L / D = 1, ε = 0.6)

Λ	Results	Without slip, Kn=0			With slip, Kn=0.1		
		$\emptyset$	W_0	P_L	$\emptyset$	W_0	P_L
0.1	1	84.76	0.1243	17.94	87.55	0.0719	13.39
	2	83.5709	0.1294	18.0281	86.4306	0.0737	13.4245
0.2	1	79.70	0.2483	17.91	85.11	0.1438	13.39
	2	76.9766	0.2608	17.9755	82.6269	0.1479	13.4242
0.5	1	66.78	0.6146	17.74	78.03	0.3592	13.39
	2	65.4832	0.6306	17.7763	74.5521	0.3652	13.4218
1	1	52.76	1.1829	17.40	67.58	0.7151	13.38
	2	51.9228	1.1995	17.4120	62.9951	0.7160	13.4158
2	1	38.56	2.1239	16.90	52.55	1.3911	13.38
	2	38.7655	2.1311	16.9104	49.3922	1.3479	13.4081
5	1	22.47	3.8259	16.23	31.84	2.9349	13.37
	2	24.0417	3.8832	16.2788	32.6115	2.7577	13.4348
10	1	13.43	4.8935	15.91	19.43	4.2399	13.35
	2	15.5070	5.2580	15.9611	22.2184	4.1596	13.4994

1: The results of Malik [30] **2: Present analysis**

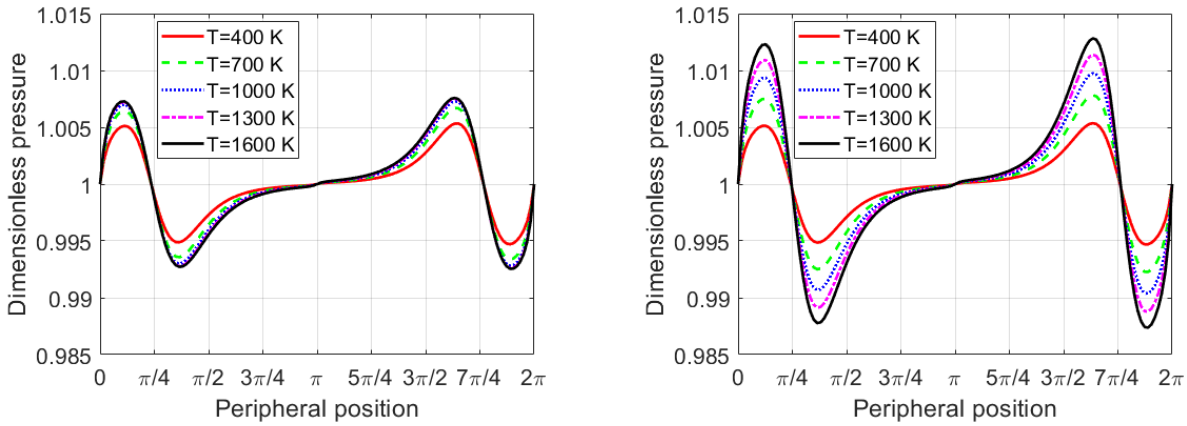

(a) (b)

Fig. 2. Pressure profile in the middle section of the two-lobe non-circular micro gas bearing - ω = 100,000 rpm, ζ = 0. (a) With rarefied effect (b) Without rarefied effect

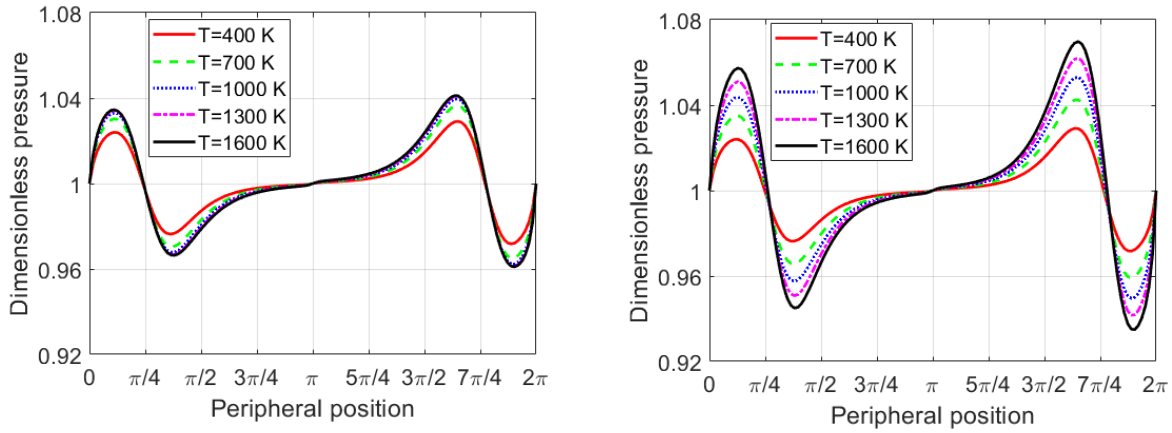

(a) (b)

Fig. 3. Pressure profile in the middle section of the two-lobe non-circular micro gas bearing - ω = 500,000 rpm, ζ = 0. (a) With rarefaction effect (b) Without rarefaction effect

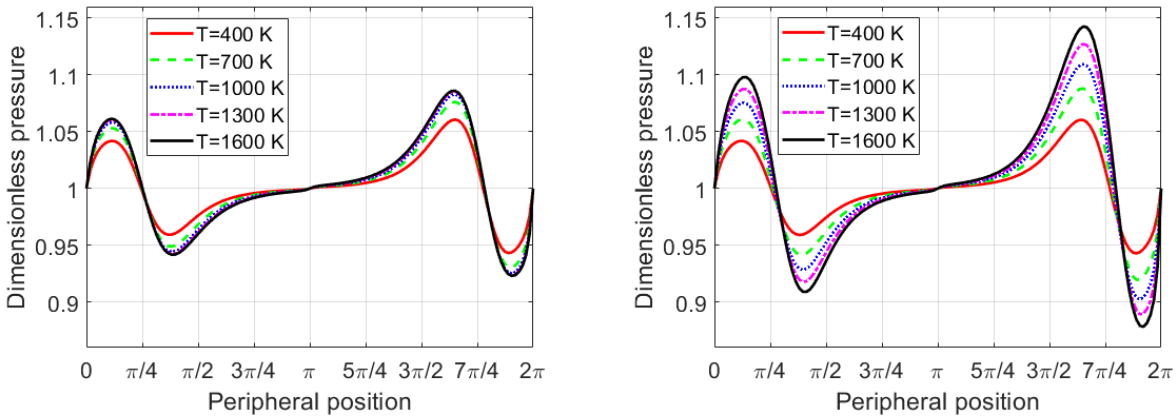

(a) (b)

Fig. 4. Pressure profile in the middle section of the two-lobe non-circular micro gas bearing - ω = 1,000,000 rpm, ζ = 0. (a) With rarefaction effect (b) Without rarefaction effect

In the case where the effect of rarefaction is considered, after 1000 K with increasing temperature, almost no increase in the amount of pressure is observed. According to the pressure diagrams in the two cases, at 400 K the amount of pressure is almost the same which shows that at low temperatures the effect of rarefaction is negligible.

Fig. 3 shows the pressure profile when the rotational speed of the rotor is 500,000 rpm in two cases. As the rotational speed of the rotor increases, the pressure values increase. When the effect of gas rarefaction is considered, the pressure values decrease. At low temperatures, the rarefaction effect of the gas film is not significant, as can be seen at 400 K, the pressure profile is almost the same in both cases. With increasing gas temperature and without considering the rarefaction effect of the gas film, the

Fig. 4 shows the pressure profile when the rotational speed of the rotor is 1,000,000 rpm in two cases. As the rotational speed of the rotor increases, the pressure values increase.

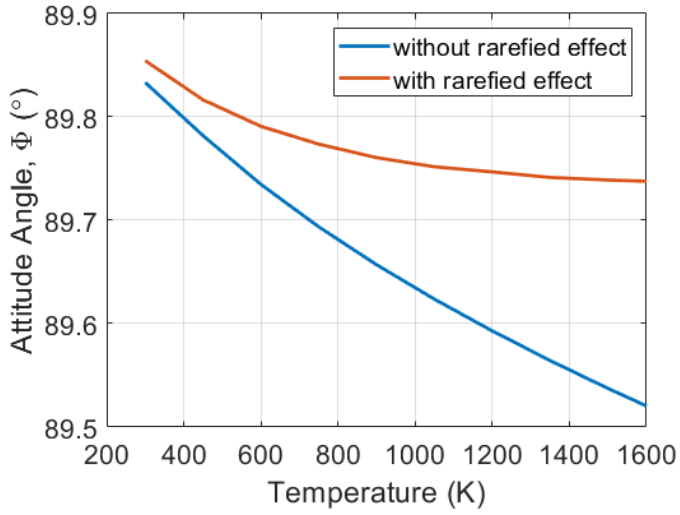

Fig. 5. The effect of temperature rise and gas rarefaction on the attitude angle - ω=100,000 rpm .

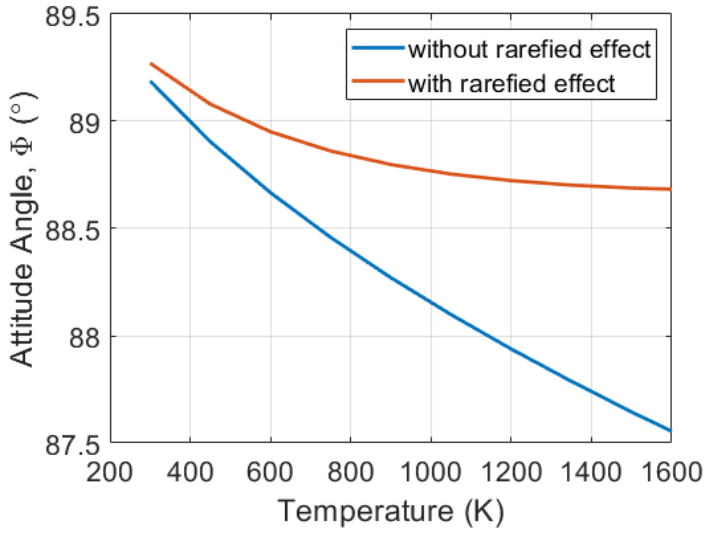

Fig. 6. The effect of temperature rise and gas rarefaction on the attitude angle - ω=500,000 rpm .

When the effect of gas rarefaction is considered, at higher temperatures, the higher the temperature, the much lower the pressure increase.

In Fig. 5, the effect of the temperature and the gas rarefaction on the attitude angle, $\varnothing$, of the two-lobe non-circular micro gas bearing has been investigated when the rotational speed of the rotor is 100,000 rpm. As can be seen, with increasing gas temperature, the attitude angle decreases, but when the gas rarefaction is considered, the attitude angle decreases with a slight slope.

In Figs. 6 and 7, the effect of the temperature and the gas rarefaction on the attitude angle, $\varnothing$, of the two-lobe non-circular micro gas bearing has been investigated when the rotational speed of the rotor is 500,000 and 1,000,000 rpm respectively. As the rotational speed of the rotor increases, the amount of attitude angle decreases. With increasing gas temperature, the attitude angle decreases, but when the gas rarefaction is considered, the attitude angle decreases with a

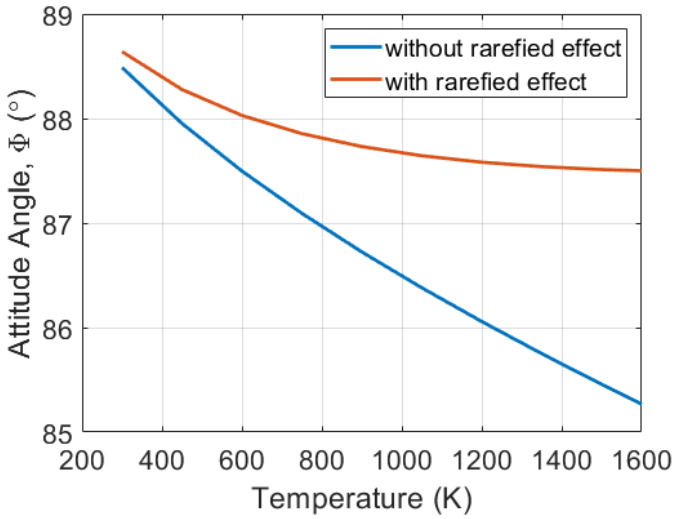

Fig. 7. The effect of temperature rise and gas rarefaction on the attitude angle - ω=1,000,000 rpm.

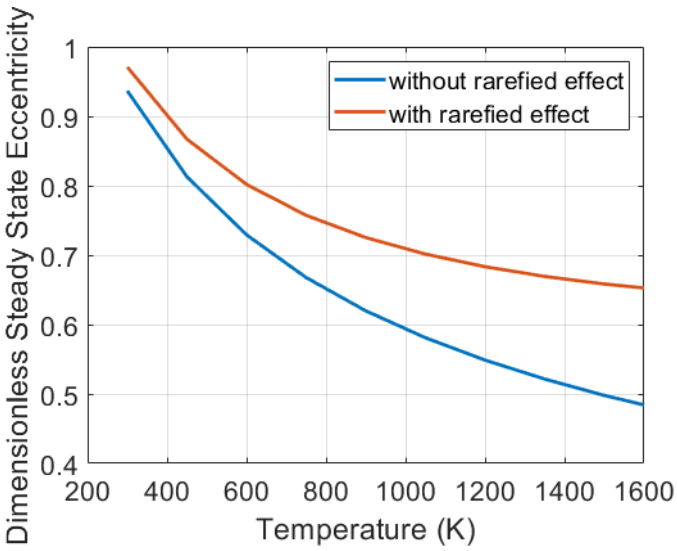

Fig. 8. The effect of temperature change and gas rarefaction on the steady state eccentricity of the journal center - ω=100,000 rpm.

smaller slope.

In Fig. 8, the effect of the temperature rise and the gas rarefaction on the eccentricity of the rotor of micro-bearing center has been investigated when the rotational speed of the rotor is 100,000 rpm. As can be seen, with increasing gas temperature, the eccentricity decreases. When the effect of gas rarefaction is considered, more eccentricity is predicted. With increasing gas temperature and without considering the rarefaction effect of the gas film, the eccentricity decreases by 46.83% and considering the rarefaction effect, this value is equal to 32.19%. At low temperatures, with the rarefaction effect, the eccentricity increases by 3.66%, which at high temperatures is equal to 32.21%.

In Figs. 9 and 10, the effect of the temperature rise and the gas rarefaction on the eccentricity of the rotor of micro-bearing center has been investigated when the rotational speed of the rotor is 500,000 and 1,000,000 rpm respectively. As the rotational speed of the rotor increases, the eccentricity

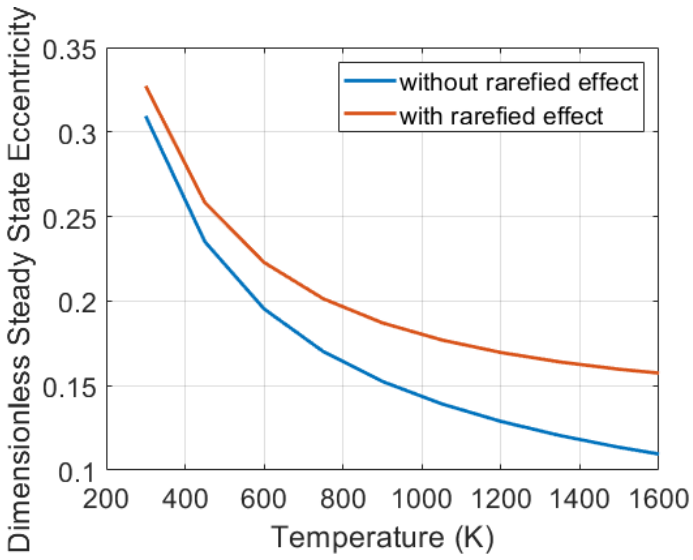

Fig. 9. The effect of temperature change and gas rarefaction on the steady state eccentricity of the journal center - ω=500,000 rpm.

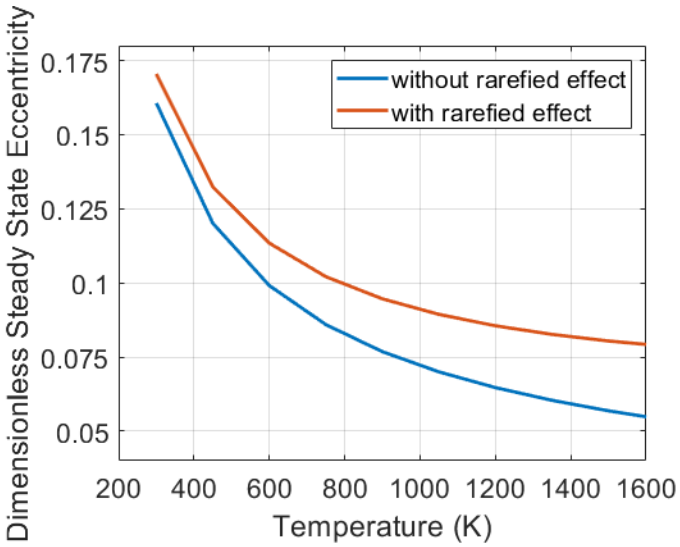

Fig. 10. The effect of temperature change and gas rarefaction on the steady state eccentricity of the journal center - ω=1,000,000 rpm.

decreases. As can be seen, with increasing gas temperature, the eccentricity decreases. When the effect of gas rarefaction is considered, more eccentricity is predicted.

In Fig. 11, the effect of the temperature rise and the gas rarefaction on the load carrying capacity of the micro gas bearing has been investigated when the rotational speed of the rotor is 100,000 rpm. As the temperature of the gas increases, the load carrying capacity of the bearing increases. When the effect of gas rarefaction is considered, a smaller amount is predicted for load bearing capacity. As the gas temperature increases, regardless of the rarefaction effect in the gas film, the load carrying capacity of the micro gas bearing increases by 184.8%. If the effect of rarefaction is considered, the increase in the load carrying capacity decreases to about 97.56%. When the rarefaction effect of the gas film is considered, the load carrying capacity decreases, with a reduction rate of about 7.9% at low temperatures and about 36.11% at high temperatures.

In Figs. 12 and 13, the effect of the temperature rise and the gas rarefaction on the load carrying capacity of the micro

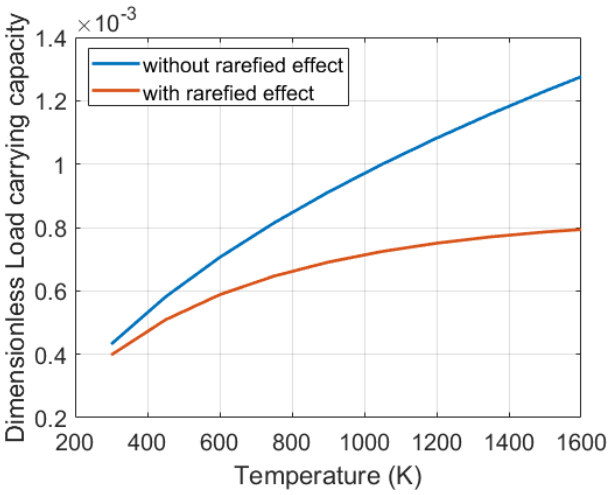

Fig. 11. The effect of temperature rise and gas rarefaction on the load carrying capacity - ω=100,000 rpm.

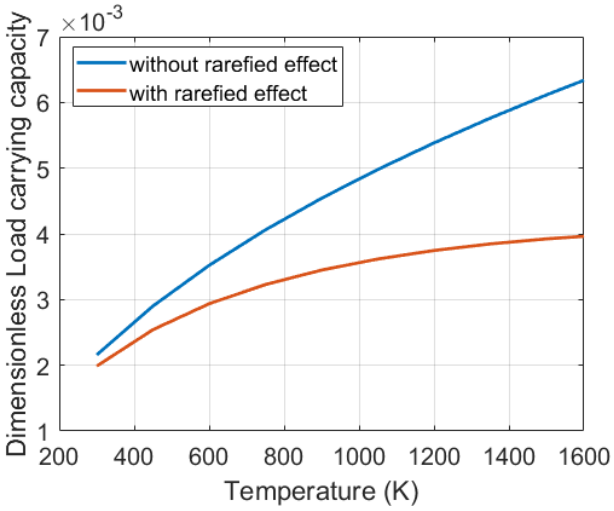

Fig. 12. The effect of temperature rise and gas rarefaction on the load carrying capacity - ω=500,000 rpm.

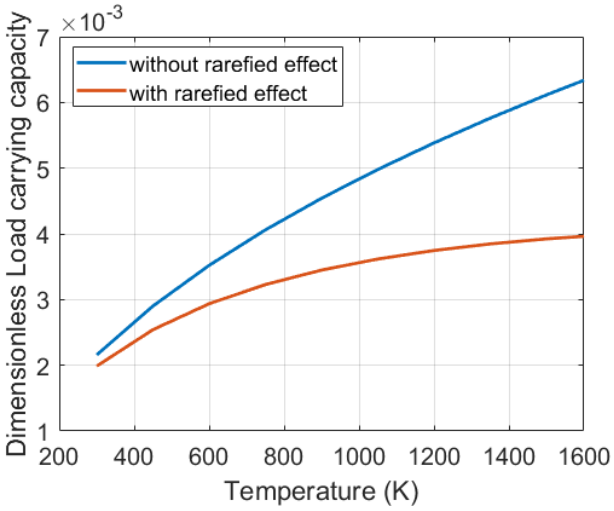

Fig. 13. The effect of temperature rise and gas rarefaction on the load carrying capacity - ω=1,000,000 rpm.

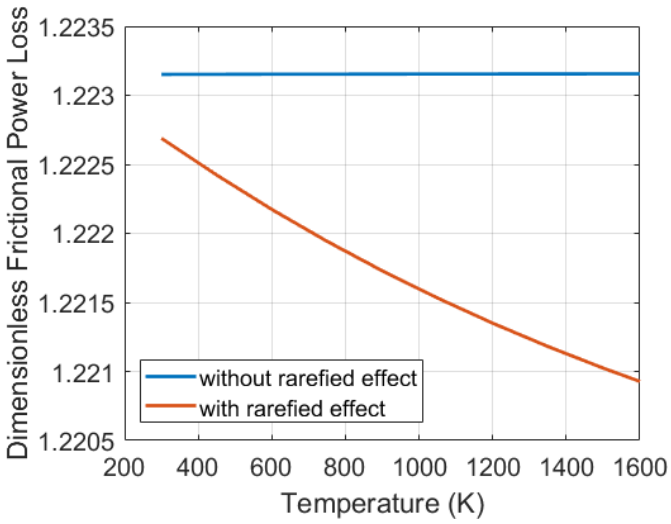

Fig. 14. The effect of temperature rise and gas rarefaction on the frictional power loss. ω=100,000 rpm.

gas bearing has been investigated when the rotational speed of the rotor is 500,000 and 1,000,000 rpm respectively. As the rotational speed of the rotor increases, the load carrying capacity increases. As the temperature of the gas increases, the load carrying capacity of the bearing increases. When the effect of gas rarefaction is considered, a smaller amount is predicted for load bearing capacity. With increasing gas temperature and without considering the rarefaction effect of the gas film, the percentage increase of the load carrying capacity in Fig. 12 is about 183.3% and in Fig. 13 is about 180.5%. The percentage increase in load carrying capacity decreases when the rarefaction effect is considered, which is about 97.3% in Fig. 12 and about 97.24% in Fig. 13. At a given temperature, taking into account the rarefaction effect, the load carrying capacity decreases, with a percentage reduction of about 7.9% at low temperatures in Figs. 12 and 13. The amount of this percentage reduction at high temperatures in Fig. 12 is about 35.84% and in Fig. 13 is about 34.74%.

In Fig. 14, the effect of the temperature rise and the gas rarefaction on the frictional power loss of the micro gas bearing has been investigated when the rotational speed of the rotor is 100,000 rpm. As the temperature of the gas increases, the frictional power losses do not change much and are almost constant, but if the effect of gas rarefaction is considered, the frictional power losses decrease with increasing temperature which the reduction percentage, in this case, is about 0.12%. Considering the rarefaction effect of the gas film, the reduction percentage of frictional power losses at low temperatures is about 0.04% and at high temperatures is about 0.16%, which indicates that at high temperatures the frictional power losses are 4 times higher than losses are at low temperatures.

In Figs. 15 and 16, the effect of the temperature rise and the gas rarefaction on the frictional power loss of the micro gas bearing has been investigated when the rotational speed of the rotor is 500,000 and 1,000,000 rpm respectively. As the rotational speed of the rotor increases, the frictional power losses are reduced. As the effect of gas rarefaction is considered, the frictional power losses decrease with increasing temperature.

5- Conclusions

In micro gas bearings, due to the need for high speeds to increase load carrying capacity, there will be a possibility of temperature rise. The high temperature and the small size of the micro-bearing will lead to a rarefaction of the gas film, and ignoring the effect of gas rarefaction in solving the Reynolds equation will result in incorrect results. In this paper, the molecular gas lubrication model is used to analyze the steady state behavior of two-lobe non-circular gas lubricated micro bearings. The effects of temperature increase and gas rarefaction on gas pressure profile, load bearing capacity, angle of attitude, eccentricity ratio and frictional power loss have been studied and analyzed. The results show that with increasing gas rarefaction, the gas pressure and consequently the load carrying capacity decrease more, and the attitude angle also increases more. Some other results are as follows:

1- As the gas temperature increases, the pressure and load carrying capacity increase and the attitude angle, eccentricity and frictional power losses decrease.

2- At a certain temperature, taking into account the rarefaction effect of the gas film, the attitude angle and eccentricity increase and the load carrying capacity and frictional power losses are reduced.

3- At high temperatures and high rotational speed:

The pressure reduction percentage is approximately 10

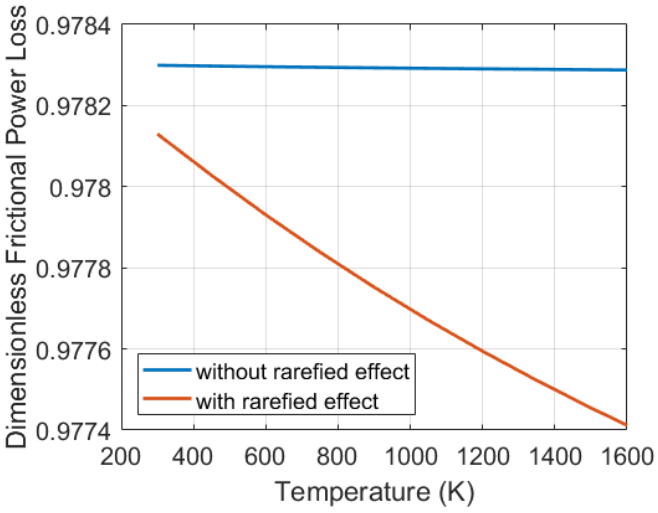

Fig. 15. The effect of temperature rise and gas rarefaction on the frictional power loss. ω=500,000 rpm .

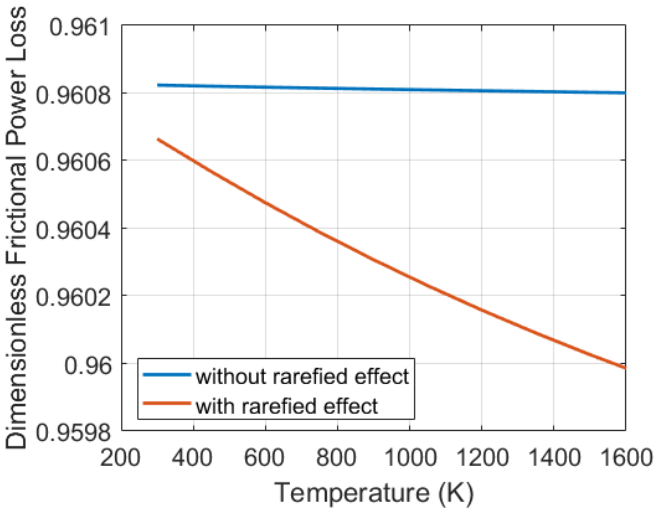

Fig. 16. The effect of temperature rise and gas rarefaction on the frictional power loss. ω=1,000,000 rpm.

times higher than the reduction percentage at low rotational speeds.

The percentage increase in attitude angle is approximately 10 times higher than the percentage increase in low rotational speed.

The percentage increase in eccentricity is 1.3 times higher than the percentage increase in low rotational speed.

The percentage reduction in load carrying capacity is approximately the same as the percentage reduction in low rotational speed.

The percentage reduction in frictional power losses is approximately half the percentage reduction in low rotational speed.

The results show that the effect of gas rarefaction has great importance and affects all the characteristics of the steady state of the two-lobe micro gas bearing.

Nomenclature

A	2-D domain of integration
C	Conventional radial clearance, m
C_m	Minor clearance when rotor and bearing geometric centers are coincident, m
D	Journal diameter, m
D_k	Inverse Knudsen number
F_e	$\bar{F}_e/p_aR^2$, The external load applied to the journal
F_x , F_y	$F_x = \frac{f_x}{p_aR^2}, F_y = \frac{f_y}{p_aR^2}$, Non-dimensional components of the gas film resultant force on the rotor
F_{gx} , F_{gy}	$F_x = \frac{f_{gx}}{p_aR^2}, F_y = \frac{f_{gy}}{p_aR^2}$, Non-dimensional components of the gas film force on the rotor
F_{fx}, F_{fy}	$F_{fx} = \frac{f_{fx}}{p_aR^2}$, $F_{fy} = \frac{f_{fy}}{p_aR^2}$, Non-dimensional components of the shear force on the rotor
F_{ex} , F_{ey}	$F_{ex} = \frac{f_{ex}}{p_aR^2}$, $F_{ey} = \frac{f_{ey}}{p_aR^2}$, Non-dimensional components of the external force on the rotor
$\bar{F}_L$	$\frac{F_L\mu R^3\omega}{C_m}$, Friction force, N
$\bar{P}_L$	$\frac{P_L\mu R^4\omega^2}{C_m}$, Frictional power loss, watt
h	$h = HC_m$, Film thickness, m
Kn	Knudsen number
L	Bearing length, m
N_i	Shape function
n_e	Number of nodes in an element
n_k	Number of nodes in fluid domain
p	$p = Pp_a$, Absolute gas pressure, $\mathrm{N/m^2}$
p_a	Ambient pressure, $\mathrm{N/m^2}$
Q	Non-dimensional flow rate coefficient
Q_c	Flow rate coefficient of continuum flow
Q_p	Flow rate coefficient of Poiseuille flow
R	Rotor radius, m
R_g	Gas constant
S	1-D domain of integration
T	Temperature, K
U	Peripheral speed of the rotor, $\mathrm{m/s}$
W_0	Dimensionless load carrying capacity
x, y, z	Cartesian axes with the origin at the bearing geometric center, m
$X_{j0}. Y_{j0}$	$X_{j0} = \bar{X}_{j0}/C_m . Y_j = \bar{Y}_{j0}/C_m$, Coordinates of the rotor center in steady state

Greek symbols

δ	Preload in the bearing, (C_m/C)
$\emptyset$	Attitude angle
Λ	Bearing number
μ	Ambient dynamic viscosity of the lubricant, pa · s
θ	Angular coordinate measured from X-axis
θ_0^k	Angle of lobe line of centers for kth Lobe
θ_1^k, θ_2^k	Angles at the leading and trailing edge of the lobe
ε	ρ/C_m , Eccentricity ratio
ω	Rotational speed of the rotor, rpm
ζ	$\zeta = z/R$, Coordinate along bearing axis measured from mid span
λ	Molecular mean free path, m

Subscript

0	Static equilibrium position of the rotor bearing

Superscript

e	Element numbers
k	Lobe designation

References

[1] E.S. Piekos, K.S. Breuer, Pseudospectral Orbit Simulation of Nonideal Gas-Lubricated Journal Bearings for Microfabricated Turbomachines, Journal of Tribology, 121(3) (1999) 604-609.

[2] D. Kim, S. Lee, M. Bryant, F. Ling, Hydrodynamic Performance of Gas Microbearings, Journal of Tribology-transactions of The Asme - J TRIBOL-TRANS ASME, 126 (2004).

[3] K. Isomura, S. Tanaka, S.-i. Togo, M. Esashi, Development of high-speed micro-gas bearings for three-dimensional micro-turbo machines, Journal of Micromechanics and Microengineering, 15(9) (2005) S222-S227.

[4] M. Arghir, S.L. Lez, J. Frene, Finite-volume solution of the compressible Reynolds equation: Linear and non-linear analysis of gas bearings, Proceedings of the Institution of Mechanical Engineers, Part J: Journal of Engineering Tribology, 220(7) (2006) 617-627.

[5] W.-M. Zhang, G. Meng, J.-B. Zhou, J.-Y. Chen, Slip model for the ultra-thin gas-lubricated slider bearings of an electrostatic micromotor in MEMS, Microsystem Technologies, 15(6) (2009) 953-961.

[6] H.-j. Zhang, C. Zhu, Q. Yang, Characteristics of Micro Gas Journal Bearings Based on Effective Viscosity, Journal of Tribology, 131 (2009) 041707.

[7] H.-j. Zhang, C.-s. Zhu, M. Tang, Effects of rarefaction on the characteristics of micro gas journal bearings, Journal of Zhejiang University-SCIENCE A, 11(1) (2010) 43-49.

[8] W.-M. Zhang, J.-B. Zhou, G. Meng, Performance and stability analysis of gas-lubricated journal bearings in MEMS, Tribology International, 44(7) (2011) 887-897.

[9] X.-Q. Zhang, X.-L. Wang, R. Liu, B. Wang, Influence of temperature on nonlinear dynamic characteristics of spiral-grooved gas-lubricated thrust bearing-rotor systems for microengine, Tribology International, 61 (2013) 138–143.

[10] J. Yan, G. Zhang, Z. Liu, F. Yang, Static Characteristics of Gas Foil Thrust Bearing Based on Gas Rarefaction Model, 2015.

[11] X. Zhang, Q. Chen, J. Liu, Steady Characteristics of High-Speed Micro Gas Journal Bearings with the Different Gaseous Lubricants and the Extreme Temperature Difference, Journal of Tribology, 139 (2016).

[12] D. Chen, S. Zhou, J. Han, J. Fan, Q. Cheng, Characteristics evaluation of gas film in the aerostatic thrust bearing within rarefied effect, Proceedings of the Institution of Mechanical Engineers, Part J: Journal of Engineering Tribology, 231(2) (2016) 149-157.

[13] L. Li, D. Zhang, Y. Xie, Probabilistic Sensitivity Analysis of Wear Property for MEMS Gas Bearing, Applied Sciences, 9(20) (2019).

[14] Y. Wu, L. Yang, T. Xu, H. Xu, Combined Effect of Rarefaction and Effective Viscosity on Micro-Elasto-Aerodynamic Lubrication Performance of Gas Microbearings, Micromachines, 10(10) (2019).

[15] Y. Wu, L. Yang, W. Wu, T. Xu, Research on Static and Dynamic Characteristics of Gas-lubricated Microbearings

for Microfluidic Devices, Applied Sciences, 10 (2020) 1634.

[16] O. Pinkus, Analysis of Noncircular Gas Journal Bearings, Journal of Lubrication Technology, 97(4) (1975) 616-623.

[17] M. Chandra, M. Malik, R. Sinhasan, Comparative study of four gas-lubricated noncircular journal bearing configurations, Tribology International, 16(2) (1983) 103-108.

[18] N. Saha, B.C. Majumdar, Study of externally-pressurized gas-lubricated two-layered porous journal bearings: A steady state analysis, Proceedings of the Institution of Mechanical Engineers, Part J: Journal of Engineering Tribology, 216(3) (2002) 151-158.

[19] A. Rahmatabadi, R. Rashidi, Effect of mount angle on static and dynamic characteristics of gas-lubricated, noncircular journal bearings, Iranian Journal of Science and Technology, Transaction B: Engineering, 30 (2006).

[20] W.A. Crosby, B. Chetti, The Static and Dynamic Characteristics of a Two-Lobe Journal Bearing Lubricated with Couple-Stress Fluid, Tribology Transactions, 52(2) (2009) 262-268.

[21] A.D. Rahmatabadi, R. Rashidi Meybodi, M. Nekoeimehr, Preload effects on the static performance of multi-lobe fixed profile journal bearings with micropolar fluids, Proceedings of the Institution of Mechanical Engineers, Part J: Journal of Engineering Tribology, 225(8) (2011) 718-730.

[22] A. Chauhan, R. Sehgal, R.K. Sharma, Investigations on the thermal effects in non-circular journal bearings, Tribology International, 44(12) (2011) 1765-1773.

[23] S.C. Sharma, V. Phalle, S. Jain, Performance of a noncircular 2-lobe multirecess hydrostatic journal bearing with wear, Industrial Lubrication and Tribology, 64 (2012).

[24] H. Shooroki, R. Meybodi, S. Karbassi, G. Loghmani, Numerical solution of Reynold's equation governing noncircular gas bearing system using radial basis function, Iranian journal of science and technology. transaction a, science, 38 (2014) 389-397.

[25] X. Chen, J.K. Mills, G. Bao, Static performance of the aerostatic journal bearing with grooves, Proceedings of the Institution of Mechanical Engineers, Part J: Journal of Engineering Tribology, 234(7) (2019) 1114-1130.

[26] S. Fukui, R. Kaneko, Analysis of Ultra-Thin Gas Film Lubrication Based on Linearized Boltzmann Equation: First Report—Derivation of a Generalized Lubrication Equation Including Thermal Creep Flow, J. Tribol., 110 (1988) 253.

[27] S. Fukui, R. Kaneko, A Database for Interpolation of Poiseuille Flow Rates for High Knudsen Number Lubrication Problems, Journal of Tribology, 112(1) (1990) 78-83.

[28] J.N. Reddy, Introduction to the Finite Element Method, Third Edition, 3rd edition. ed., McGraw-Hill Education, New York, 2006.

[29] X.-Q. Zhang, X.-L. Wang, L.-N. Si, Y.-D. Liu, W.-T. Shi, G.-J. Xiong, Effects of Temperature on Nonlinear Dynamic Behavior of Gas Journal Bearing-rotor Systems for Microengine, Tribology Transactions, 59 (2016).

[30] M. Malik, Theoretical Considerations of Molecular Mean Free Path Influenced Slip in Self-Acting Gas-Lubricated Plain Journal Bearings, Proceedings of the Institution of Mechanical Engineers, Part C: Journal of Mechanical Engineering Science, 198(1) (1984) 25-31.

HOW TO CITE THIS ARTICLE

A. Gharanjik, A. Karami mohammadi, Effects of gas temperature rise on steady state behavior of non-circular two-lobe micro gas bearings, AUT J. Mech Eng., 5(3) (2021) 343-360.

DOI: 10.22060/ajme.2021.18654.5910